Cover Page

Universiteit Leiden

The handle http://hdl.handle.net/1887/20251 holds various files of this Leiden University dissertation.

Author: Kumar, Manohar
Title: A study of electron scattering through noise spectroscopy
Issue Date: 2012-12-05

3

EXPERIMENTAL SETUP: DESIGN AND TECHNIQUES

The smallest nanoscale systems such as atomic chains and single molecule bridges show rich physical properties. They form test-beds for probing concepts in quantum transport. Among the experimental techniques scanning tunneling microscope and mechanically controllable break junctions have been extensively used to study such systems. The mechanically controllable break junction technique used here is based on thinning down to single atom a macroscopic wire having a weak link at the center by mechanical force. Once a single-atom contact is formed the physical properties of the system are dominated by quantum mechanics. The coupling of this atom with the bulk metal can be controlled at the sub-Ånsgstrom level, giving an opportunity to tune the quantum properties of the system. This simple set up forms the platform for our studies of the quantum properties of one-dimensional quantum system such as atomic chains and single-molecule junctions. In this chapter we are introducing the basic terminology, concepts and experimental techniques which we have used in further chapters.

3.1 THE MECHANICALLY CONTROLLABLE BREAK JUNCTION TECHNIQUE

THE mechanically controllable break junction (MCBJ) technique for the study of atomic-size junctions was developed by Muller *et.al.* [1] in Leiden, based upon an earlier design that Moreland and Ekin *et.al.* [2] used for the study of the tunnel current through vacuum between Nb electrodes. The design is very simple and basically consists of a metal wire with a weak link in the center. It is placed on top of a bendable substrate. The wire is stretched at its weakest link by bending the substrate using a mechanical screw mechanism. A schematic of such a design is shown in figure (3.1). Once the wire is broken, the distance between the two ends of the freshly cleaved lead can be further controlled mechanically. The vertical dis-

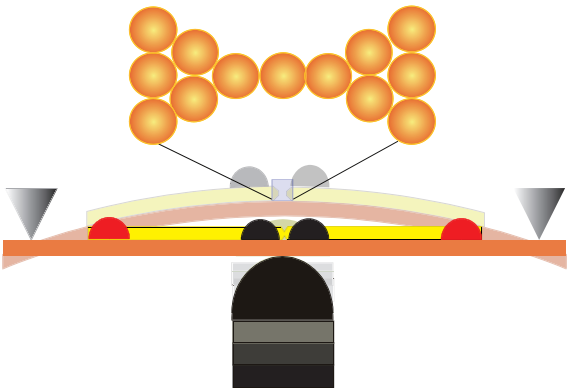

FIGURE 3.1: Schematic of the mechanically controllable break junction technique: A sample wire is fixed on top of a bendable substrate using epoxy glue (black droplets). An atomic-scale contact is formed using fine control by a piezo-electric drive (black cylindrical rod) in a three-point bending configuration.

placement of the mechanical drive δz produces a lateral displacement δd at the weak link of the wire that is much smaller due to the small stretching of the substrate surface with the bending. The ratio of the lateral displacement with respect to the vertical displacement gives the attenuation factor of the MCBJ set up, which is also called the reduction ratio[3]. This factor r is given as:

$$r = \frac{\delta d}{\delta z} = \frac{6tu}{L^2}, \tag{3.1}$$

where t is the thickness of the substrate, u is the length of the wire between the anchoring points, and L is the length of the sample between the counter supports.

For the sake of reference let us calculate the reduction ratio for a typical MCBJ sample. The typical numbers for the parameters in (3.1) are $t = 1$mm, $u = 0.1$mm and $L = 20$mm, which gives $r \approx 1 \times 10^{-3}$. The significance of this number can be understood considering the example of a mechanically feasible displacement $\delta z = 0.1\mu$m for which δd is about 0.1Å. This is about $1/25^{th}$ of the atomic diameter of a Au atom. Hence, the spatial resolution of the MCBJ control is much smaller than the inter-atomic distance. This spatial resolution can be further improved using a piezoelectric element to push the bendable substrate. A spatial resolution well below $1pm$ can be obtained in this way. [1]

Two types of break junctions

The MCBJ can be classified into two different types, that are illustrated in figure (3.2) :

Notched wire break junctions : This type of break junction is quite commonly used for metals other than Au. It uses a wire having a notch carved in the center. Usually the notch in the wire is made by means of a surgical knife. At the notch the diameter of the wire is reduced to 25%–50% of its original diameter. The wire is fixed upon a kapton covered phosphorous bronze substrate using epoxy adhesive. A top layer of kapton tape acts as the insulator between the sample wire and the phosphorous bronze substrate. The two epoxy anchoring points around the notch should be very close to the notch in order to have better stability and higher spatial resolution. The sample is left curing for a day and then is mounted an the three point bending configuration of the mechanical drive system. The junction is broken first using a mechanical screw, but once the sample is broken the piezo element is used to fine tune the distance between the two freshly cleaved surfaces[1].

Lithographic break junction : This type of break junction is made by electron beam lithographic processes and is almost exclusively used for Au metal electrodes. The sample wire is formed by thermally evaporating a high purity metal film directly on a polished bendable substrate, that is planarized by spincoating of a polymer layer, often polyimide. The notch in the junction is formed using electron beam lithography, and a freely suspended bridge is formed by a step of isotropic ion etching, which attacks the polyimide under the metal film. The lithographic junction is first broken and controlled by means of a mechanical gear and an electromotor drive[5].

[1] For measurement of the electrode displacement one needs to calibrate each sample individually [4].

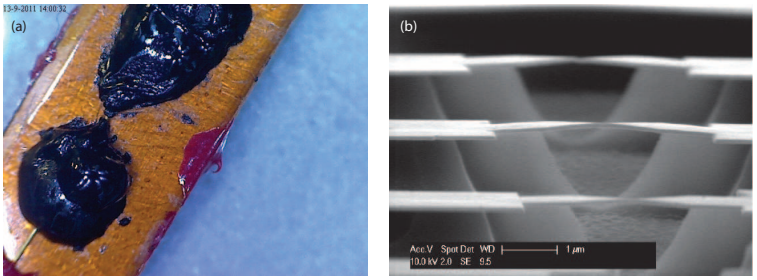

FIGURE 3.2: Left: Photograph of a notched wire break junction. Right: SEM image of lithographically fabricated break junctions; in this case three are formed on the same substrate (courtesy C.A. Martin [6]).

Each of the above two MCBJ methods has its own advantages and disadvantages. The lithographic junctions have a better stability and their distance resolution is at least three orders of magnitude better than the notched wire break junction. The much smaller reduction ratio gives a stability of the order of 10^{-5}Å$/min$. This permits characterizing the atomic system for longer periods of time without drift in the contact. The stability for the notched wire MCBJ is $1-2$ orders of magnitude smaller than the above mentioned value but is still quite sufficient for longer duration junction characterization. Below we will show that this stability allows us to measure the noise on Au atomic chains over $2-3$ hours without any discernible drift in the contact. The most important disadvantage of the lithographic junctions is the fact that statistical measurements are much more time consuming. Since for lithographic break junctions the reduction ratio is too small for a piezo-electric element to have much effect, an electromotor is used for making and breaking of the contact. This process is quite slow in comparison to notched wire break junctions, where a series of rapid voltage ramps on the piezo permits collecting a histogram of 1000 breaking traces in a matter of minutes.

The main disadvantage of above two techniques is that the actual topography of the contact is not observed during the junction characterization. Some contacts show quite stable configurations and some can form very long atomic chains, while the same contact after reforming could snap. It is not very practical to work with the single crystals in the MCBJ. A SEM image of various contacts which we have used for the work in this thesis is shown in figure (3.3). Even the same sample at different stages of the making and breaking processes forms microscopic structures giving completely different properties. Generally, Au atomic contacts show much more stable contacts in comparison to ferromagnetic atomic contacts. The difference is related to the structures seen from the SEM images. Au has a much

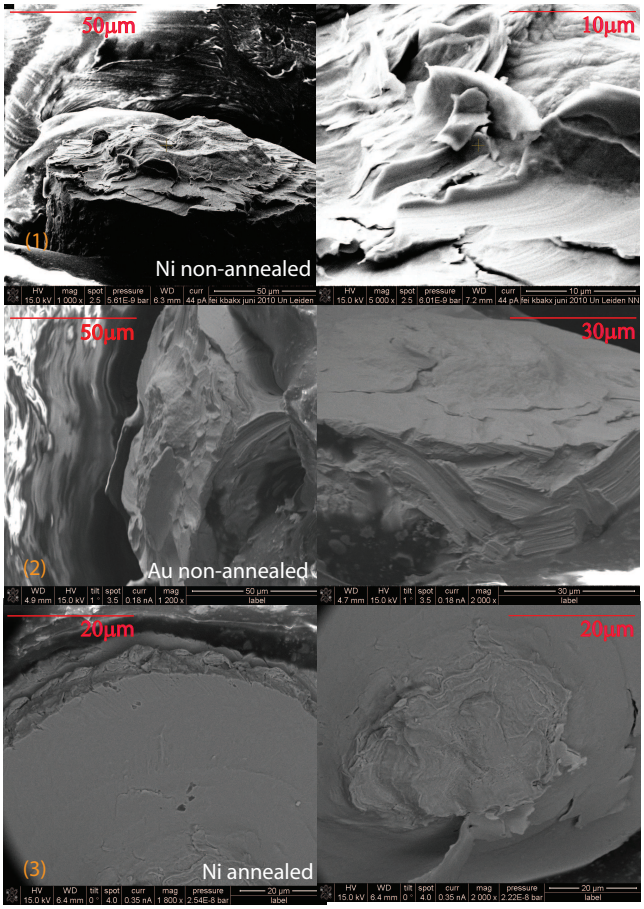

FIGURE 3.3: SEM images of different MCBJ: Scanning tunneling microscope images of the the broken surface for six different MCBJ samples. There is a drastic difference between the surface topography of Ni and Au wires. Generally, non-annealed Ni wires show a strong drift in the contact conductance. The annealing of the wire gives increased stability of the contact[2]. The SEM image of annealed Ni contacts shows less flakes in the contact region, but note that the configuration which is involved in the atomic contact formation cannot be identified in the SEM image. This is a clear disadvantage of MCBJ over STM measurements.

smoother notch area while Ni has lots of flakes in the notch area. Annealing of the Ni sample wires improves the stability of the contact by removing the granularity near the contact. Note that in these SEM images the real atomic configuration

of the contact point is missing, which determines the actual geometry determining the different physical properties of the contact. Scanning tunneling microscope has the advantage over MCBJ that it allows scanning the topography of the surface and precisely controlling and manipulating the atomic structure. Nevertheless, due to the extreme stability and to the possibility of producing atomically clean contacts gives MCBJ an edge over STM and makes it suitable for our research work. In our studies we have used the notch wire break junction technique. A photograph of one of our samples is shown in figure (3.2).

3.2 MCBJ INSERT

MCBJ experiments were done in cryogenic vacuum at helium temperatures. The MCBJ sample was mounted in a custom-made home-designed dipstick. The top of the dipstick, called the head, contains a vacuum coupling for the pumping line and several electrical feedthroughs. The bottom of the dipstick, called the sample chamber, hosts the sample. All electrical wires at the connections inside the head of the dipstick were soldered using flux and lead free soldering tin. The vacuum couplings were mainly sealed by O-rings except from those feedthroughs which needed to be baked out, which were Swagelok type. A schematic layout of the lower part of the dipstick is shown in figure (3.4). The head and bottom of the dipstick are connected by a long hollow tube of 48mm in diameter and 1.2m long, which holds several hollow tubes inside it. These small tubes are used for the wiring and are anchored to the interior wall of the dipstick, using silver welding for better thermal coupling. A Cu-Ni alloy was used for the wiring inside the dipstick for optimized electrical conduction combined with poor thermal conduction. All the wires running from the top of the dipstick are coupled to a Cu cold plate which is in contact with the He bath through a cold finger. Cu wires were used from this cold plate for connections to the sample. This differential wiring scheme helps us to keep the sample decoupled from the room temperature heat bath.

Along the center of the tube a 1.1m long mechanical axis runs from the head to the sample chamber. This axis is made of a hollow stainless steel tube in order to reduce the heat load on the He bath and the sample. On the top of the dipstick this mechanical axis is connected to a $1:100$ gear box that is attached through a Rikagou magnetic feedthrough [8]. This gear box gives us sub-micron resolution for the z-axis movement of the mechanical rod. At the lower end of this axis a fork-blade structure is mounted to allow decoupling the axis from the sample chamber. The extension of the axis at the cryogenic side is connected to a differential screw. A piezo electric element is mounted with epoxy adhesive to the bottom of the differential screw. The advantage of this design is that the mechanical axis can be used for breaking of the sample at cryogenic temperatures. Once the sample is

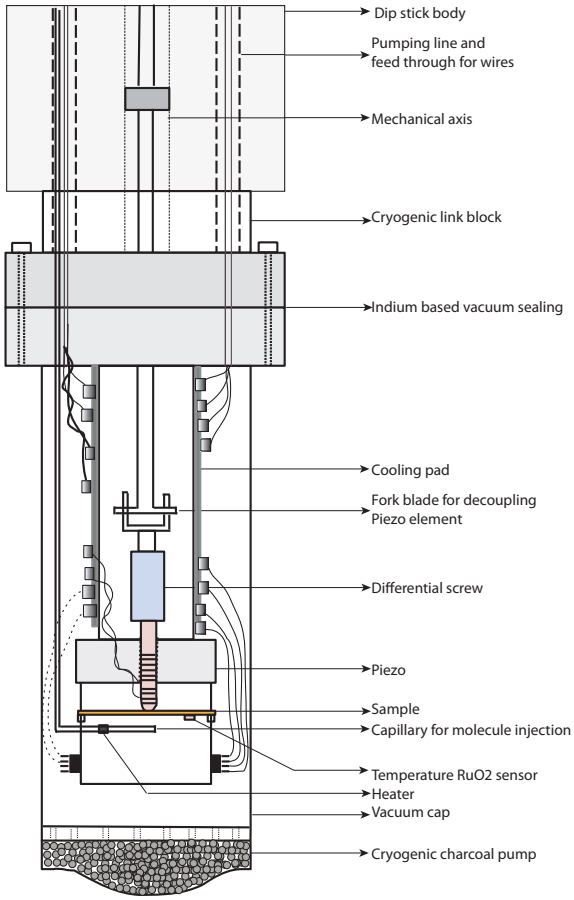

FIGURE 3.4: Schematic of the dipstick used for MCBJ experiments. The different parts of the dipstick and sample chamber are shown and labeled. The head of the dipstick is connected to the sample chamber through a long hollow tube which contains several smaller tubes for wiring and for the introduction of gas molecules in the sample chamber.

broken the axis is decoupled from the lower end using the fork and blade configuration. With the axis decoupled the piezo element can be used for fine tuning the inter-electrode distance. In this way the atomic contact is maximally decoupled from mechanical vibrations coming from the top of the dipstick. A stainless steel capillary tube of 6mm in diameter runs from the head of the dipstick to the sample chamber, and ends in a detachable nozzle. This tube we use for introduc-

ing the lighter molecules to the atomic contact. The capillary tube is fitted with a vacuum-sealed heater wire running inside the tube. The nozzle has an orifice facing the sample wire. A heater wire is mounted on the nozzle to heat it when introducing the gas while the sample is at cryogenic temperatures. The whole capillary and nozzle are thermally isolated from the He bath. On the top of the dipstick the capillary is connected to a needle valve through a Swagelok connection. The advantage of this design is that the whole capillary can be baked out without damaging the wire connections and other vacuum sealing. In order to measure the temperature of the capillary tube during bake out process, several Pt-10K resistive thermometers are placed along the tube. The nozzle is fitted with a Pt-100K resistor. A 10K $Ru0_2$ resistor is used for measuring the temperature of the sample. A four-probe wire connection is preferred for the $Ru0_2$ thermometer for accurate temperature measurement of the sample. The other resistance thermometers are fitted with a 2-wire measurement scheme. The sample holder is clamped to the dipstick through a screw mechanism and vacuum sealed by an indium seal. The cryogenic cap of the dipstick is fitted with a compartment filled with Norit activated carbon which acts as a cryogenic pump.

The dipstick is pumped using a two-stage pump system. For rough pumping a rotary pump is used and, once the base pressure of the dipstick is approximately 10^{-3}mbar, it is further pumped using a turbomolecular pump. The dipstick is pumped to a pressure of 10^{-5}mbar, as measured at the top of the dipstick. Once this pressure is reached the capillary is baked out for a day. After the baking the base pressure improves to $10^{-6} - 10^{-7}$mbar. Next, the dipstick is cooled down in the liquid nitrogen first and then lowered into liquid He^3. Once the dipstick is in the liquid He the cryogenic pump overtakes the turbo pumping, hence all the valves on the top of the dipstick are closed, apart from the capillary valve. With the dipstick closed the cryogenic vacuum is expected to be well below 10^{-10}mbar, but this was not measured directly.

3.3 THE ELECTRONIC CIRCUIT

THE electronic circuits employed in our setup can be divided into three independent circuits: (a) The conductance measurement (ac and dc) setup. (b) Piezo biasing circuit. (c)The noise measurement setup. The schematic of our conductance measurement circuit is shown in figure (3.5). We have employed a two-probe measurement technique for the conduction measurement. The dc voltage biasing is provided from a National Instruments data acquisition card (DAQ-NI 6221). NI DAQ provides a digital to analog convertor with 16 bit digital accu-

[3] The two-step cooling is followed in order to reduce the liquid He consumption; one can also cool down the dipstick first in cold He gas and dip it gradually in the liquid He bath.

racy. The current is measured through a current/voltage converter and one of the analog-to-digital inputs of the data acquisition card. For point contact spectroscopy an ac modulation signal of 2mV amplitude and a frequency of 3.33kHz was added, as obtained from the generator in a SR830 lockin amplifier. In this lockin measurement technique a reference signal is used to modulate the dc bias signal. The lockin amplifier takes the signal from the sample, multiplies it with the reference signal, integrates it over a specified time constant, and gives a signal proportional to the harmonics of the reference (see below, equation(3.2)). The lockin amplifier can extract the phase and amplitude information of a signal in a noisy environment. The lockin measurement technique is used to detect small changes of about 1% in the signal with an accuracy better than 1%. The overall accuracy of ac conductance measurement was checked using fixed calibration resistors. The resistance measured in our setup is within 1% of the four probe measurement value. We have two switches (S1 and S2) for the coupling and decoupling of the conductance measurement with the noise measurement circuit. The S1 is used to short the sample while S2 decouples the ac signal from the sample. The dc measurement setup is used to characterize the junction by measuring the conductance breaking/making traces while the ac measurement is done to study the smaller signals like the perturbation in the current due to electron-phonon coupling.

The potential on the piezo element is controlled using the DAQ. The signal from the DAQ is amplified using a homemade high voltage amplifier. Special attention is taken to decouple the ground of the piezo element from the common ground of the dipstick. The noise measurement setup is discussed below, in the section (3.5.1)

3.4 THE CHARACTERIZATION OF ATOMIC CONTACTS

THE MCBJ technique can attain a distance resolution of sub-Ångstrom level with a stability of 10^{-5}Å$/min$. It being very simple the MCBJ technique is a strong tool to investigate the properties of individual atoms in the contact. Once the wire is broken to the point where only single atom is bridging between the two bulk leads the physical properties of the system are dominated by the species at the center of the contact. To investigate the properties of this atom in detail, it is needed to characterize the atomic contact first.

3.4.1 DC CONDUCTANCE CHARACTERIZATION

The most obvious way to characterize the contacts is to look into the evolution of the current while stretching the contact. It is evident that one could see an increase in the resistance while pulling and, hence, one could expect a gradual decrease in the conductance upon increase in the distance. This is correct when the wire is still

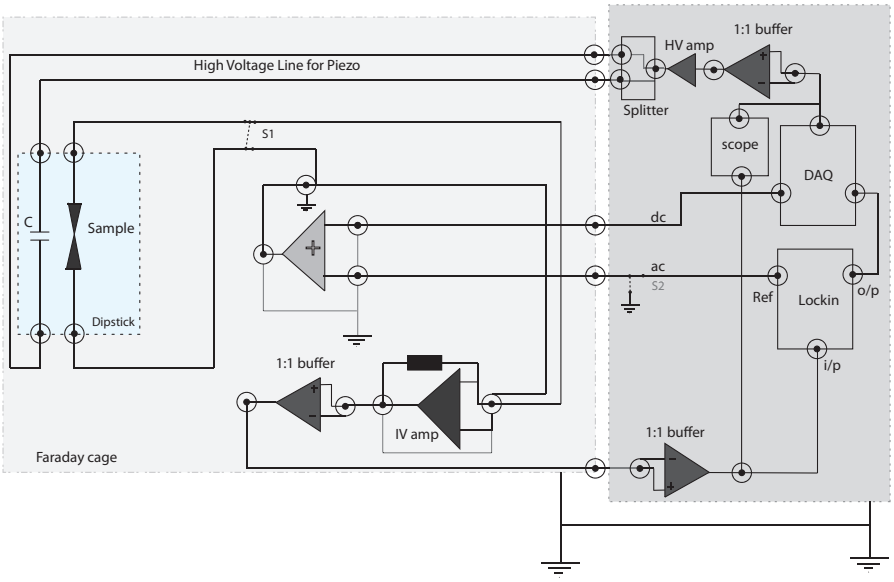

FIGURE 3.5: Schematic of the conductance circuit used in our measurement. A two-probe measurement technique is used to measure the conductance of the atomic contact. For ac measurements a lockin technique is used. The ac signal is added to t he dc signal using a home made adder. The current from the circuit is converted back to voltage using an I-V converter with variable gain. The output of the IV converter is fed into the lockin to measure the first harmonics.

in the bulk regime but when the cross section of the wire is reduced to a few atoms diameter one should expect sudden changes in the conductance due to movement of individual atoms. A few typical traces recorded on Au atomic contacts is shown in figure (3.6 a). It is remarkable to see that the conductance indeed reduces in a step fashion upon stretching of the contact. This step-wise conductance variation should not be confused with conductance quantization as in experiments on 2-dimensional electron gases [9, 10]. In our experiment the conductance follows from the step-wise variation in the atomic configuration of the contact. This is also the reason why the traces do not show regular and reproducible quantization in the conductance plateaus. Another remarkable feature to be noted here is that there is a long plateau forming just before the conductance vanishes. This long plateau can be understood in terms of the formation of perfectly well coupled regular structure upon stretching. One could ask why such structure be could formed and especially around the quantum of resistance. The presence of this structure at the quantum of resistance implies that our system has already entered into the

quantum domain, where the resistance does not depend upon diffusive scattering of the electrons by the lattice structure, but only at the interface of the quantum system with the bulk structure. These structures have been studied in detail by Yanson *et al.*[11] who have shown that these structures are in fact one dimensional atomic chains. Au and Pt are among the few metals which form atomic chains. Experimentally, van den Brom *et al.*[12] have demonstrated that Au atomic chains carry a single conductance channel. Hence, in the trace shown in figure (3.6 a) is explained by the formation of a single channel Landauer conductor a few atoms long.

Returning to the traces, one can see that it is difficult to predict the evolution of the traces, which depends upon the local atomic configuration of the leads. Hence one needs statistical averaging over atomic contact configurations. Two types of statistical analysis on conductance traces have been developed: one based on the conductance scale, the other on the piezo voltage scale. The first statistical study gives the frequency of occurrence of the conductance values, which is called the conductance histogram. A conductance histogram constructed from the recordings of 8000 Au atomic contact breaking traces is shown in figure (3.6 b). The conductance histogram shows predominantly a sharp peak at $0.98G_0$ and broader peaks at higher conductances. This is a characteristic of Au atomic contacts. Regardless of the measurement technique and for all samples Au atomic contacts always show a sharp peak around $1G_0$. In the same way histograms for Pt atomic contacts show a broad peak at $1.5G_0$. Deviations of the peak from the observed value indicates the presence of foreign atoms or molecules in the contact. The second statistical study gives information of the frequency of occurrence of the breaking voltage. The breaking voltage is the piezo voltage at which the atomic contact is broken into the tunneling regime. This type of statistics gives information on the length of chain formation. Looking at figure (3.6 c) we can see the presence of multiple peaks. This shows that occurrence of lengths of the atomic structure is not smooth, but it is discrete. The first peak is attributed to the breaking of a dimer contact, and subsequent peaks represent the breaking of atomic chains with additional atoms in the contact. This length histogram is recorded for the last plateau only. The last plateau corresponds to the first peak in the conductance histogram which signifies a contact of a single atom in cross section. For Au length histograms are recorded for sections of the conductance traces between $G_{min} = 0.85G_0$ and $G_{max} = 1.05G_0$. These parameters vary for different atomic species.

For a correct determination of the chain length one needs to calibrate the reduction ratio of the contact. One of the methods proposed by Muller *et al.*[13] is based on measurement of the tunneling current as the function of the inter-electrode distance. The tunneling current decays exponentially with increasing inter-electrode distance. The logarithmic derivative of this function gives a mea-

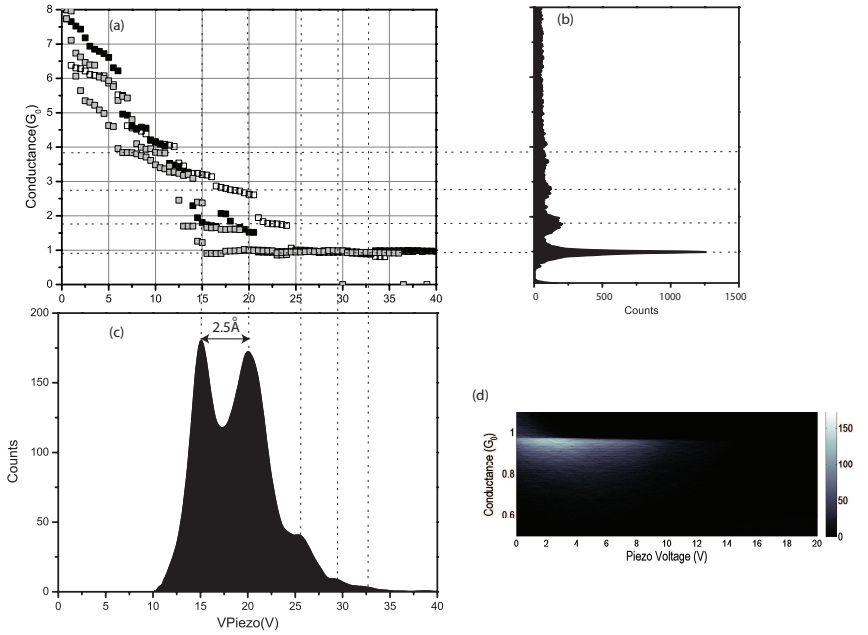

FIGURE 3.6: Characterization of atomic contacts for Au. (a) Three examples of dc conductance traces recorded for Au atomic contacts. The biasing voltage used to record the trace was 80mV. The conductance traces show the formation of a long last plateau formation upon stretching of the contact, after which the contact breaks into the tunneling regime. The traces shown here are a few selected traces showing the presence of the 4-5 atom long atomic chains. (b) A statistical representation of the frequency of occurrence of conductance values during breaking of the contacts. This conductance histogram was recorded for values between $0.1G_0 - 8G_0$. For Au atomic contacts the histogram shows a prominent peak at $0.98G_0$. (c) Histogram of the lengths of last plateaus for the breaking of atomic contacts. For Au, it shows the probability for long chain formation with peaks at regular distances suggesting an origin in the atomic spacing. The length histogram was recorded for conductance values between $1.05G_0 - 0.85G_0$. The first peak corresponds to a 2 atom contact and subsequent peaks correspond to chains having additional atoms in the contact. (d) The combination of the conductance histogram and the length histogram in the form of a 2D density plot. For construction of the plot 8000 conductance traces were taken.

sure of the reduction ratio. This procedure is not very precise due to the dependence of the tunneling current on the work function, which explicitly depends upon the atomic configuration of the leads. Another more sophisticated approach uses Gundlach oscillations, *i.e.* the oscillations in the tunneling resistance in the field emission regime. Here, we rather use a simpler approach to calibrate the reduction ratio for our samples, as proposed by Untiedt *et al.* [4]. Using their number

for the inter-atomic distance between Au atoms in a chain is 2.5Å, a comparison with the distance between the peaks in the length histogram gives for the reduction ratio $r = 5.0/2.5 = 2.0V/Å$.

3.4.2 AC CONDUCTANCE MEASUREMENT

The dc conductance characterization can accurately verify the cleanliness of the atomic contacts. However, this method cannot identify the exact nature of the species in the contact. The dc measurements are done at fixed bias, but the conductance varies with bias, depending on the nature of the species in the contact and its coupling with the leads, on the presence of vibration modes and on local atomic configurations of the leads. Hence, probing this bias dependence gives valuable information, not only about the nature of the atomic species but also its coupling to the leads. The vibration mode signal is quite small, typically of the order of $1-2\%$ of the zero-bias conductance. Hence, the common method to reveal this signature is to measure the differential conductance using a lockin technique, or by numeric derivatives of the current. For lockin measurements the dc signal is modulated by a small ac signal. Lockin measurements give a much better signal-to-noise ratio through detection of the harmonics of the conductance. This can be seen from a Taylor expansion of the modulated signal $I\left(V_b^{dc} + V_m^{ac}\cos(\omega t)\right)$ up to second order.

$$\begin{aligned} I\left(V_b^{dc} + V_m^{ac}\cos(\omega t)\right) &= I(V_b) + \left|\frac{dI}{dV}\right|_{V_b} V_m \cos(\omega t) + \frac{1}{2}\left|\frac{d^2I}{d^2V}\right|_{V_b} V_m^2 \cos^2(\omega t) \\ &= I(V_b) + \left|\frac{dI}{dV}\right|_{V_b} V_m \cos(\omega t) + \frac{1}{4}\left|\frac{d^2I}{d^2V}\right|_{V_b} V_m^2 (1+\cos(2\omega t)) \end{aligned} \tag{3.2}$$

There are two broad classes of ac conductance spectroscopy: (a) Point contact spectroscopy, which refers to the studies of inelastic scattering of electrons in the ballistic regime of metallic point contacts, and (b) Inelastic electron tunneling spectroscopy, which refers to study of inelastic scattering of electrons in the tunneling regime.

Inelastic electron tunneling spectroscopy

In systems like metal-molecule-metal junctions the metal electrodes often can be regarded as separated through a tunneling gap. If the voltage applied across the molecular junction is such that $eV \geq \hbar\omega$, for an given vibration mode energy $\hbar\omega$ then there is a certain probability that the electron will interact with the vibration mode of the molecule. This interaction leads to forward scattering of the electron with a reduced energy of $E_F + eV - \hbar\omega$. This can be understood as the opening

of a new inelastic channel. In the differential conductance this can be seen as an increase in the conductance at the threshold energy [14].

Point contact spectroscopy

Point contact spectroscopy (PCS) was introduced by Yanson *et al.*[15] in the early 1970's. In the ballistic regime electrons traverse a junction without any scattering. However, at higher bias there is a finite probability of electron to be scattered by vibration modes at the contact. The probability for backscattering of the electrons depends upon the ratio $(a/d)^2$ where a is the radius of the constriction and d the distance to the center of the contact. Hence the backscattering of the electrons takes place within a spherical volume of radius a. The early works of Yanson *et al.* and others[15–17] on metallic point contacts concluded that PCS can be used as a tool to identify the phonon density of states of the metals, or more precisely, the spectrum of electron-phonon scattering strength.

In case of atomic contacts a is the radius of a single atom, hence the volume of electron backscattering is small. This also implies that electrons scatter back from a single lattice distance, or within the atomic contact. Hence, point contact spectra for atomic contacts show local vibration modes rather than bulk phonons. The strength of this inelastic signal is on the order of 1% which can be easily hidden in the conductance fluctuations that result from interfering electron waves[18]. These conductance fluctuations can be understood in terms of partial reflection and transmission of electron waves at the contact. If there is single transmission channel in a contact and there is a finite probability that the electron is reflected from the contact this reflected wave could undergo multiple partial reflections. As long as the total path of the reflected electron is within the coherence length of the electron the partial waves superimpose with the transmitted partial wave. The phase accumulated along a path of length L can be written as kL where k is the momentum of the interfering electron wave, which is voltage dependent. This gives an bias-dependent interference signal in the differential conductance.

These conductance fluctuations are dependent on the transmission probability τ of the atomic contact. In the limit of $\tau \simeq 1$ the amplitude of conductance fluctuations is negligible, but for other values they may mask the vibration mode signal. This is the main limitation of PCS in atomic contacts. Since for Au the s electrons form a perfectly transmitting single conductance channel its easier to obtain the vibron signal in the differential conductance. However, this is not case for Pt atomic contacts, where more than one channel is present and some of the channels are partially transmitting, giving rise to stronger conductance fluctuations. Also for Au for some of the contacts our vibronic signal is hidden inside these conductance fluctuations. For vibronic frequency signal analysis it helps to compare the differential conductance with its symmetric component. The sym-

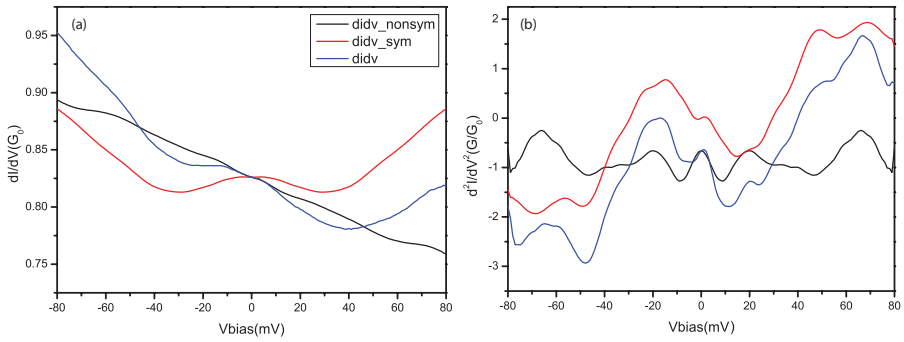

FIGURE 3.7: Characterization of Au atomic contacts by ac conductance measurements. (a) The blue curve shows the differential conductance. The symmetric component of the differential signal is computed as $G_{sym}(+V) = G_{sym}(-V) = [G(+V) + G(-V)]/2$ and shown as the red curve. A broad vibronic step down can be seen in the differential conductance at about ±15mV but this is completely overtaken by the asymmetric component $G_{nonsym}(V) = G(V) - G_{sym}(V)$ which is plotted in black color. (b) The derivatives of the corresponding differential conductance of panel a. Comparing the features in the second derivative of the current and in its symmetric component the vibronic energy is similar but shifted by asbout 3meV. This difference is incorporated in error analysis.

metric component is calculated using $G_{sym}(+V) = G_{sym}(-V) = [G(+V)+G(-V)]/2$. Figure (3.7) shows one of the worst examples where the vibronic signal is almost hidden in the background of conductance fluctuations. We included the shift in the vibronic signal of the differential conductance and its symmetric component in the error analysis. The symmetric component shows the presence of a vibronic step down feature in the signal, which is expected for a contact with $\tau = 0.83$. The second derivative of the current shows the fist peak (minimum) at $v_+ = 12$meV at positive bias while the corresponding peak at opposite bias sits at $v_- = 15$meV. In a well-coupled atomic chain with symmetric biasing the vibronic signal should be the same for positive and negative bias. Although a shift due to conductance fluctuations is likely, the discrepancy could also be due to asymmetric coupling of the atomic chain with the two leads. Hence, the symmetrized signal does not give the correct answer, and in order to obtain an estimate of the accuracy of the vibronic energy we use the difference between the two in our error analysis.

3.5 SHOT NOISE

SHOT noise in electrical conductors arises due to the discreteness of the electronic charge. It becomes prominent in quantum systems such as quantum dots, tunnel junctions and atomic contacts. In a quantum conductor with an eigen channel with transmission probability $\tau \sim 1$ shot noise is significantly reduced.

But if the transmission probability $\tau \neq 1$ electrons traversing the quantum system will be partially reflected and partially transmitted. The partial occupation of forward and backward traveling states gives rise to shot noise in the quantum conductor. The measurement of shot noise gives information on the number of the eigen channels taking part in the conductance[4]. Here we concentrate on low-frequency noise measurements for atomic contacts and singe molecule junctions.

3.5.1 SHOT NOISE MEASUREMENT CIRCUIT

We have employed a cross spectrum analysis technique for the noise measurements. The signal that we need to measure is of the order of $1\text{nV}/\sqrt{\text{Hz}}$ which is comparable to the noise of the best low-noise amplifiers available. In case of Au atomic contacts $1/f$ noise is very low, and starts to dominate only below 20kHz for bias values above 25meV. This is why we can use a low-frequency noise measurement setup, up to 100kHz, for this system. For single molecule junctions $1/f$ noise is much higher and we have developed a noise measurement technique with a frequency window extending to 10MHz for this purpose, which we will describe in chapter "A high-frequency noise measurement setup for MCBJ". A schematic of our low-frequency noise measurement circuit is shown in figure (3.8). The voltage signal across the sample is measured differentially using two amplifier chains in parallel. The first stage is formed by the low-noise preamplifier LI75A of gain 100, which is further amplified by an EG&G amplifier of gain 1000. The amplified signals are fed to a SRS-785 two-channel spectrum analyzer. In differential ac mode the input voltage noise and current noise of the LI75A is $1.4\text{nV}/\sqrt{\text{Hz}}$ and $10\text{fA}/\sqrt{\text{Hz}}$, respectively. The input noise of the EG&G is $4\text{nV}/\sqrt{\text{Hz}}$. In this two-channel measurement scheme we can see that the noise added by the LI75A is crucial, since it is of same order as the voltage noise signal of $1.89\text{nV}/\sqrt{\text{Hz}}$ for a junction of $1G_0$ at 5K. The current noise, which we cannot suppress by the cross spectrum (equation(2.5), is just $0.13\text{nV}/\sqrt{\text{Hz}}$ the same junction, which is still small in-comparison to our voltage noise signal. The main constraint comes from the amplifier voltage noise and its coupling to our measurement signal through intrinsic capacitance of the coax, as illustrated in figure (2.3). The bandwidth of our noise measurement setup is 100kHz, but due to the high impedance of the sample and the high intrinsic cable capacitance (typically ~ 350pF) of the coax running down the dipstick to the sample chamber, the noise spectra show a low-pass roll-off at 35kHz for a junction of $1G_0$. Due to this low-pass roll-off the noise signal level at the higher frequency end (typically around 80kHz) hits the noise level due to the residual correlations. This adds to the error in our noise measurements. Typically, the error in

[4] Shot noise measurement on the quantum conductors only helps to fix the transmissions for two channels, in some cases for 3 channels. See section (Shot noise analysis) for more details.

the noise measurements is on the order of 4%.

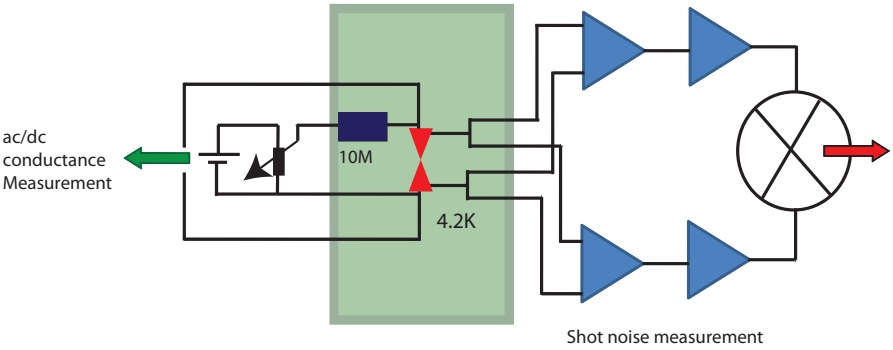

FIGURE 3.8: Schematic of the two-channel cross spectrum shot noise measurement circuit. The voltage across the sample is measured differentially using two sets of preamplifiers. The combined gain of first and second stage amplifiers is $10,000X$. The amplified signal is fed into the two-channel FFT spectrum analyzer. The cross spectrum of the two channels and the FFT of the individual channels are measured with frequency resolution of 250Hz. Averaging over 10,000 spectra takes about 2 minutes. A pseudo current-biasing scheme was used to bias the sample. Initially we have used a battery in parallel with a potentiometer to set the bias. This biasing scheme was later changed to a computer controlled voltage bias system with third order low-pass filters, with a cut off at $f_c = 3$Hz. All amplifiers are battery powered. All noise measurements were done in a shielded environment[19].

3.5.2 DESIGN RULES FOR NOISE MEASUREMENT

The noise measurement can be difficult and cumbersome. Few basic rules should be strictly followed for successful noise measurement techniques. These rules are listed below:

* ***Wiring***: Short shielded coaxes should be used for all electrical connections. Cables connected to the same hot point should be twisted to avoid the electromagnetic field pickups. Wires in the cryostat should be properly anchored and thermalized.

* ***Biasing***: Biasing of sample should be done either by battery manually or using computer. In case of using computer controlled instrument as biasing source, filtering of the spurious noise from the computer should be taken care of. Ground of the computer should be separated from the sample ground.

* ***Filtering***:All DC lines which are coupled directly to the sample especially for high frequency measurement noise should be filtered. The cryostat and

all low noise sensitive equipment like amplifiers should be placed inside a Farady cage to shield the measurement from stray electro-magnetic fields like 50Hz. Usually, transformer steel is considered as the best element for a Faraday cage. All noisy equipment like spectrum analyzers and monitors should be kept outside the Faraday cage. All the components in the Faraday cage should be battery operated.

* ***Ground***: Star ground connection is preferred and the star point should be in the cryostat. Dirty ground should be separated from the clean ground. If samples are biased using the computer then the common signal from the computer should be separated using isolation amplifiers.

* ***Cleanness***: All the wires should be labeled and properly tied up. High power lines, pumps and power transformers should be placed at a distance from Faraday cage. Non connected cables should be dismounted from the connectors. Back ground noise should be measured and characterized properly such that the origin of unwanted signals appearing on the measurement spectra can be identified.

* ***Measurement***: All measurements should be done in a noiseless environment. Usually in the night, the measurements are better when surrounding equipment is turned off. The cryostat should be held by acoustic dampers and all low frequency vibration coupling to the sample should be avoided.

Above all, one should be patient with the noise measurement, especially while measuring noise on atomic contacts which requires a quite noiseless environment. It requires long integration times and it is better to make use of automation but regular manual input is needed for checking the coupling of the external environment with the measurement. All the control parameters like the gain of amplifier and the temperature of the sample should be measured regularly to keep tab on its change.

3.5.3 SHOT NOISE ANALYSIS

For the analysis of the shot noise we measured the ac conductance of the atomic contact, and the temperature of the sample using a 10kΩ RuO_2 resistor. This helps us to determine the expected thermal noise of the sample. The noise was measured at zero bias, for obtaining the thermal noise, at a series of bias voltages in steps of typically 5mV. At the end of the shot noise measurement series, thermal noise and ac conductance of the contact is measured again. The ac conductance and thermal noise measurements at the beginning and the end of the shot noise

measurement act as checks on the stability of the contact during the noise measurement. We only considered data for which the change in the thermal noise and zero bias ac conductance during the whole noise measurement process was within 2%. We will show one of the noise measurement sequences for Au contacts below to illustrate the analysis technique.

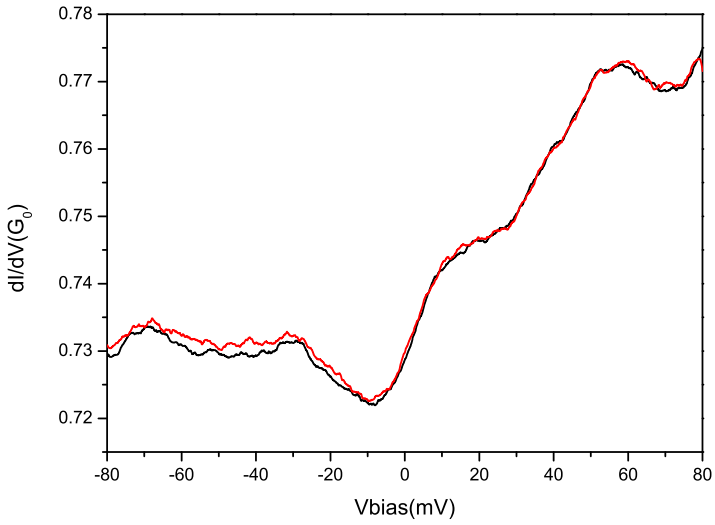

FIGURE 3.9: Differential conductance of the Au atomic used in the example shot noise measurement. The conductance of the Au atomic contact was measured at the beginning (black) and at the end (red) of the noise measurement sequence. The two are exactly same apart from the small deviation at the negative bias. The zero bias conductance agrees within the accuracy at in both differential conductance measurements.

A Au atomic contact is formed in the cryogenic environment using breaking by the piezo element. Once the stability of the contact was checked, the ac conductance of the Au atomic contact was measured using the lockin measurement technique. An ac sinusoidal signal of amplitude 2mV and frequency 2.777kHz was used to modulate the dc signal. Figure (3.9) shows the ac conductance measured at the beginning and at the end of the Au measurement run. The zero bias conductance $G(V) = 0.725G_0$ for both measurements and the shape of the curve has not changed. This shows that the contact was stable during the noise measurement. In the negative bias regime a small deviation between the two measurements can

be seen. This could be due to a very small change in distance between the two electrodes. The voltage at which this change is observed is irrelevant for the noise that is measured at much lower bias voltage. The asymmetric differential conductance feature is attributed to conductance fluctuations by interfering electron paths in the contact.

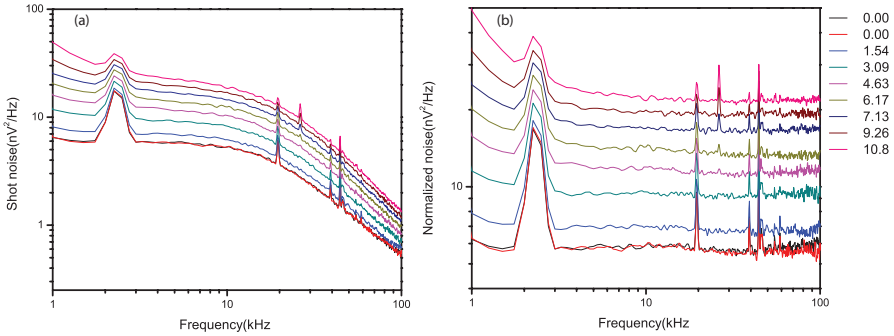

FIGURE 3.10: Noise spectra for a Au atomic contact. (a) Raw noise data measured on a Au atomic contact of conductance $0.725G_0$. The spectra were measured at different bias voltages in steps of approximately 1.5mv. The spike at about 2.5kHz corresponds to the lockin signal; other higher frequency spikes around 20,26,39, and 45kHz correspond to stray signals picked up from the oscilloscope and from the Wheatstone bridge for thermometer measurement. (b)The spectra are corrected for the low-pass behavior by normalizing to the thermal noise and correcting for the mean thermal noise value. The spectra show the some $1/f$ noise at lower frequency, but are nicely flat above 10kHz. The labels in the index show the biasing voltage(mV) used for the noise spectra. The color indexes in both panels are the same.

Noise spectra measured for this contact are shown in figure (3.10). The thermal noise measured on the contact corresponds to a temperature of 6.21K which agrees within the experimental accuracy with the thermometer reading of 6.3K obtained from the RuO_2 resistor. The thermal noise shows a roll-off with a corner frequency of 25kHz. This roll-off agrees within the accuracy with that expected for a stray capacitance of 350pF and conductance of $0.725G_0$. We present spectra in in the range $1-100$kHz because below 1kHz the contribution of $1/f$ noise becomes prominent. A range of the noise spectrum far from the $1/f$ noise corner frequency is selected for further noise analysis. For this particular case the $1/f$ noise corner frequency is below 1kHz and the range between $20-80$kHz was selected for the analysis. We have seen that The spikes seen in the spectra do not reflect intrinsic properties of the atomic contact and they were removed manually. The corrected and spikes-removed spectra are shown in figure (3.11). For each bias setting the mean noise value over the selected frequency range, and its standard deviation normalized to the number of frequency bins, was calculated as shown in figure (3.11 a). This stan-

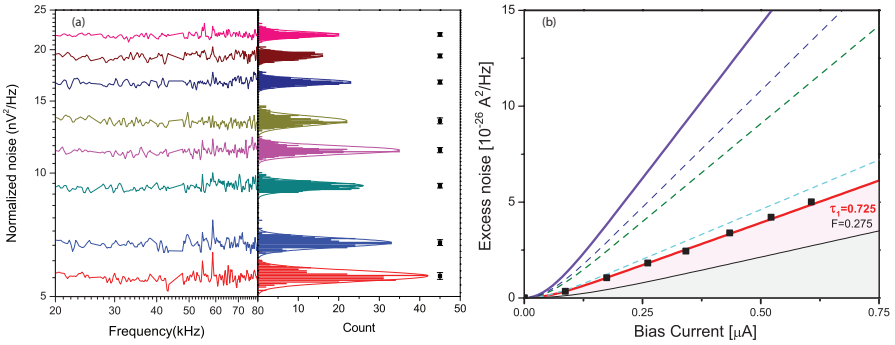

FIGURE 3.11: Shot noise analysis for a Au atomic contact. (a) Normalized spectra for the Au atomic contact data in figure (3.10) , limited to the range 20 – 80kHz, with the spikes removed. The histogram for these spectra gives the mean values of the noise and standard deviations. (b) The mean current noise values with their accuracies are plotted w.r.t. the corresponding biasing parameter. The violet curve shows the full shot noise behavior, $S_I = 2eI$, while the red curve shows a fit to the Lesovik-Levitov expression (1.28). The corresponding Fano factor is 0.275, which agrees with a transmission $\tau = 0.725$ expected for a single conductance channel and a conductance of $0.725G_0$. The light blue dashed curve is the Lesovik-Levitov (1.28) noise for a hypothetic two-channel conductor with $\tau_1 = 0.7$ and $\tau_2 = 0.025$, which lies well above the experimental data points. The Fano factor for this case is $F = 0.323$. This shows the sensitivity of shot noise for the channel composition in the atomic contact. The green dashed line is the Lesovik-Levitov noise(1.28) for $\tau_1 = 0.362$ and $\tau_2 = 0.363$ giving a Fano factor of $F = 0.637$. The more the transmission value moves towards $\tau = 0.5$, the higher the noise. The blue dashed curve is the Lesovik-Levitov noise(1.28) for three equal channels giving a Fano factor of $F = 0.758$; the higher the number of channels the larger the noise. The red curve is, in fact, the minimum level of noise for a conductor of $G = 0.725G_0$. The pink shaded region is inaccessible for spin degenerate electrons. The black curve shows the minimum noise level for the case that spin splitting of the channels is allowed ($\tau_\uparrow = 1$ and $\tau_\downarrow = 0.45$). The black shaded region is inaccessible for any kind of Landauer conductor.

dard deviation gives a measure of the accuracy of the mean value. The mean current noise value is calculated from the voltage noise $S_I(V) = S_V(V) \cdot G^2$. The mean current noise power is plotted *w.r.t.* the corresponding current bias as shown in figure (3.11 b). The experimental data points are fit to the Lesovik-Levitov expression(equation(1.28)) with a single transmission channel value of $\tau = 0.725$, which corresponds to Fano factor of $(1 - \tau) = 0.275$. The Fano factor agrees with the conductance of $0.725G_0$. The data clearly confirm that Au atomic contacts form single channel Landauer conductors. This is consistent with previous noise measurements on Au atomic contacts by van den Brom *et al.* [12] and to calculations of the number of channels in Au atomic contacts by Scheer *et al.*[20] This measurement also serves as a calibration for our noise setup.

In this analysis, we need to fit the transmission probability of the channel iteratively which is cumbersome. Figure(3.12) shows the analysis based on equa-

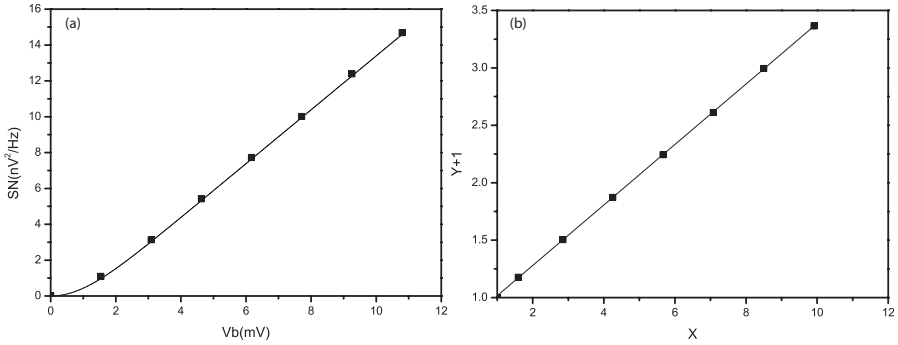

FIGURE 3.12: Reduced axis shot noise analysis. The experimental data points are plotted in the reduce axis format (right panel) and the slope of the linear fit of the experimental data points gives a Fano factor of 0.271 ± 0.02. The error here is standard deviation of the fit of the slope. The Fano factor obtained equals the expected value for a single channel Landauer conductor, $F = 1 - G$, to within the experimental error of 1% in the conductance measurement. Using this Fano factor, the noise values in the standard plot (left panel) are shown to be well-described by the Lesovik-Levitov expression(equation(1.28)).

tion (1.29). The experimental noise values are plotted using the reduced axis plot, where $Y = \frac{S(V)}{S(0)} - 1$ and $X = \left[\frac{eV}{2k_BT}\coth\left(\frac{eV}{2k_BT}\right)\right]$. The slope of this plot immediately gives the Fano factor, $F = 0.271 \pm 0.02$, which is close to value of 0.275 obtained by above technique[5]. The Fano factor calculated from the reduced axis plot is used to produce the curve from the Lesovik-Levitov expression (equation(1.28)) which correctly describes the experimental data points. Note that we are plotting the voltage noise instead of the current noise. We follow this analysis in remainder of this thesis.

In the figure (3.11 b) we show a curve for the full shot noise, $S_I = 2eI$ (violet curve). This is the maximum noise one could see in in a Landauer conductor, and it corresponds to a Fano factor of 1. Any observation of noise above this curve, *i.e.* $F > 1$, implies the presence of positive correlations in the electron transport in the contact, which is super-Poissonian noise. Any noise below this curve, *i.e.* $F < 1$, is sub-Poissonian noise. The noise we found for our contact is at the minimum noise level for a spin degenerate Landauer conductor. The pink region below this curve is inaccessible for a spin degenerate conductor. Data points in this region would indicate the presence of the spin split channels in the conductor. The black curve is the minimum noise for the case when spin degeneracy of the transmission

[5]The two values agree within the experimental accuracy limit when we consider the error of 1% in the conductance.

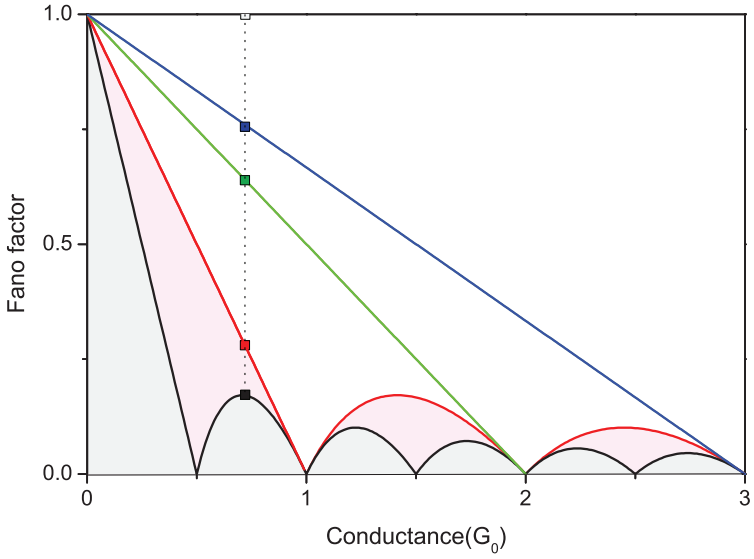

FIGURE 3.13: Fano plot for Landauer conductor. This figure is the generalized form of figure (3.11 b). The color code is kept the same. The black curve is the minimum noise level for a spin-split Landauer conductor as a function of the total conductance. The light-grey region is inaccessible to any kind of Landauer conductor. The red curve is the minimum noise for a spin-degenerate Landauer conductor. Data points in the light pink region signify the presence of the spin splitting. The green and blue lines show the maximum level of noise for two and three channels, respectively. For the reference the Fano factors discussed in figure (3.11 b) are represented as dots here. The black dot gives the point on the minimum Fano curve once spin degeneracy is lifted, ($F = 0.17$), the red dot is for the experimental Fano factor, *i.e.* $F = 0.275$, the green dot is for the presence of two equally open channels, $F = 0.638$ and the blue dot is for three equally open channels, $F = 0.758$. The white dot gives the full shot noise with the Poissonian value and $F = 1$. This plot helps in determining the number of channels in a Landauer conductor. Any solution above the green line requires more than 2 channels and cannot be uniquely determined.

channels is lifted. The light grey region is inaccessible for any kind of Landauer conductor.

This concept can be generalized to all conductance values. Figure (3.13) shows this generalized concept. Here, the Fano factor in different limiting cases is plotted with respect to the conductance value. The black curve is the minimum Fano factor for a conductor with spin-split channels. The grey shaded region is inaccessible for any kind of conductor. The red curve is the minimum noise level for a spin-degenerate conductor. The green line is the maximum noise for a two-channel Landauer conductor (four spin channels). Any conductor having a Fano factor ly-

ing above this green line signifies the presence of at least three channels taking part in the conduction. The blue line is the maximum noise for three channels taking part in the conduction (six spin channels). The presence of any data point between the red curve and the green line implies the presence of at least two channels in the conductor and presence of a data point between the green and the blue line shows the presence of at least three channels taking part in the conduction.

These are the solutions for a Landauer conductor imposed by the relations $F = \sum_{i=1}^{N} \tau_i(1-\tau_i)/\sum_{i=1}^{N} \tau_i$, $G = \sum_{i=1}^{N} \tau_i$ and $\tau_i \in [0,1]$. Any data points above the red curve does not have a unique solution. When assuming the numbers of channels are limited to 2 or 3, information that may be derived from calculations, more restricted solutions may be obtained. Hence, in this thesis we focus on our finding at low Fano factors.

REFERENCES

[1] R. J.M.Krans and C.J.Muller and I.K. Yanson, Th.C.M. Govaert and J. Ruitenbeek, *One atom point contacts*, Physical Review B **48**, 14721 (1993).

[2] J. Moreland and J. W. Ekin and L. F. Goodrich and T. E. Capobianco and A. F. Clark, *Break-junction tunneling measurements of the high-T c superconductor*, Physical review Rapid Communications **35**, 8856 (1987).

[3] A. I. Yanson, Ph.D. thesis, Universitiet Leiden (2001).

[4] C. Untiedt, a. Yanson, R. Grande, G. Rubio-Bollinger, N. Agraït, S. Vieira, and J. van Ruitenbeek, *Calibration of the length of a chain of single gold atoms*, Physical Review B **66**, 1 (2002).

[5] J. M. van Ruitenbeek, A. Alvarez, I. Pineyro, C. Grahmann, P. Joyez, M. H. Devoret, D. Esteve, and C. Urbina, *Adjustable nanofabricated atomic size contacts*, Review of Scientific Instruments **67**, 108 (1996).

[6] C. A. Martin, D. Ding, H. S. J. van der Zant, and J. M. van Ruitenbeek, *Lithographic mechanical break junctions for single-molecule measurements in vacuum: possibilities and limitations*, New Journal of Physics **10**, 065008 (2008).

[7] I. K. Yanson, O. I. Shklyarevskii, J. M. van Ruitenbeek, and S. Speller, *Aluminum nanowires: Influence of work hardening on conductance histograms*, Phys. Rev. B **77**, 033411 (2008).

[8] H. Walter, Tech. Rep., Rigaku Vacuum Products USA (2002).

[9] D. A. Wharam, T. J. Thornton, R. Newbury, M. Pepper, H. Ahmed, J. E. F. Frost, D. G. Hasko, D. C. Peacock, D. A. Ritchie, and G. A. C. Jones, *One-dimensional transport and the quantisation of the ballistic resistance*, Journal of Physics C: Solid State Physics **21**, L209 (1988).

[10] B. J. van Wees, L. P. Kouwenhoven, H. van Houten, C. W. J. Beenakker, J. E. Mooij, C. T. Foxon, and J. J. Harris, *Quantized conductance of magnetoelectric subbands in ballistic point contacts*, Physical Review Letters **38**, 3625 (1988).

[11] A. I. Yanson, G. R. Bollinger, H. E. van den Brom, N. Agrait, and J. M. van Ruitenbeek, *Formation and manipulation of a metallic wire of single gold atoms*, Nature **395**, 783 (1998).

[12] H. van den Brom and J. van Ruitenbeek, *Quantum Suppression of Shot Noise in Atom-Size Metallic Contacts*, Physical Review Letters **82**, 1526 (1999).

[13] C. Muller, J. van Ruitenbeek, and L. de Jongh, *Experimental observation of the transition from weak link to tunnel junction*, Physica C: Superconductivity **191**, 485 (1992).

[14] J. Lambe and R. C. Jaklevic, *Molecular Vibration Spectra by Inelastic Electron Tunneling*, Phys. Rev. **165**, 821 (1968).

[15] I. K. Yanson, *Non Linear effects in electric-conductivity of point junctions and electron-phonon interaction in normal metals*, Sov. Phys. JETP **39,**, 1974 (1974).

[16] S. R. I. Kulik I. O., Moskalets M V and Y. I. K, *Spectroscopy of Electron-Phonon Interaction in Point Contacts with a Barrier Layer*, JETP Lett. **50**, 1989 (49).

[17] A. G. M. Jansen, F. M. Mueller, and P. Wyder, *Normal Metallic Point Contacts*, Science **199**, 1037 (1978).

[18] B. Ludoph and J. M. v. Ruitenbeek, *Conductance fluctuations as a tool for investigating the quantum modes in atomic-size metallic contacts*, Phys. Rev. B **61**, 2273 (2000).

[19] Helko Elbert van den Brom, Doctoral thesis, Leiden university, Leiden (2000).

[20] Elke Scheer and N Agräit and J C Cuevas and A Levy Yeyati and B Ludoph and Martin-Rodero Alvaro and G R Bollinger and J van Ruitenbeek and U Cristian, *The signature of chemical valence in the electrical conduction through a single-atom contact*, Nature **394**, 154 (1998).